Three-dimensional convection in a horizontal fluid layer subjected to a constant shear

By R. M. CLEVER AND F. H. BUSSE

Institute of Geophysics and Planetary Physics, University of California at Los Angeles, CA,
USA *and* Institute of Physics, University of Bayreuth, 858 Bayreuth, Germany

Rayleigh–Bénard convection in the presence of a plane Couette flow is investigated by numerical computations. From earlier work it is well known that longitudinal rolls are preferred at the onset of convection and that at Prandtl numbers of the order unity or less these rolls become unstable with respect to the wavy instability which introduces wavy distortions perpendicular to the axis of the rolls. In the present analysis the three-dimensional flows arising from these distortions are studied and their stability is considered. A main result is the subcritical existence of three-dimensional flows at Rayleigh numbers far below the critical value for onset of convection.

1. Introduction

Thermal convection in a fluid layer heated from below and subjected to a mean shear represents a basic problem of geophysical fluid dynamics. Because of its obvious importance for the dynamics of the atmosphere this problem has long been investigated by theoretical meteorologists (Asai 1970; Kuettner 1971) and others. From the early work of Gallagher & Mercer (1965) it is known that rolls aligned with the direction of the shear represent the preferred mode for the onset of small-amplitude convection. Unlike convection in the presence of Poiseuille flow, in which case transverse rolls may be preferred for sufficient high Reynolds numbers, the preference of longitudinal rolls in plane Couette flow is independent of the Reynolds number because of the stability of isothermal plane Couette flow with respect to infinitesimal disturbances. This situation is changed when finite-amplitude disturbances are considered. As is well known for the isothermal case, and as will become apparent for the stratified case of plane Couette flow from the analysis of the present paper, there is a considerable region of the parameter space where subcritical onset of finite-amplitude instabilities occurs.

The original motivation of the present work arose from the work of Clever, Busse & Kelly (1977, referred to in the following as CBK) on the instabilities of longitudinal rolls in plane Couette flow. It is apparent from that work that even at relatively small supercritical Rayleigh numbers and small Reynolds numbers the longitudinal roll solution is unstable with respect to the wavy instability which tends to bend the rolls in a periodic fashion along their axis. The primary goal of the following analysis is the study of the steady three-dimensional convection flows arising from the wavy instability.

The subject of convection in the presence of shear has been treated extensively in the literature and a comprehensive discussion of numerical computations and their relationships to experimental studies can be found in the recent paper by Domaradzki

& Metcalfe (1988). Computations of three-dimensional convection in the presence of a constant shear have usually been restricted to the Prandtl number of air and have been carried out at Rayleigh numbers in excess of 10^4, where convection is time dependent. In this paper we focus on lower Rayleigh numbers, for which steady three-dimensional flows can be obtained which do not seem to have been studied in previous work. We also investigate the stability of the steady solutions and consider the dependence of the problem on the Prandtl number.

The paper starts with the mathematical formulation of the problem in §2 and briefly discusses the wavy instability of two-dimensional longitudinal rolls in §3. Results for three-dimensional wavy rolls evolving from the wavy instability are presented in §4 for several Prandtl numbers. Because of the subcritical nature of the three-dimensional solutions in a wide range of the parameter space it becomes possible to obtain them even at vanishing or negative values of the Rayleigh number as will be shown in §5. A limited stability analysis is described in §6 and in special cases the time-periodic solution evolving from the instability is analysed. The paper closes with some concluding remarks in §7.

2. Mathematical description of the problem

We consider a horizontal fluid layer between two horizontal rigid plates separated by a constant distance d and moving in opposite directions. Constant temperatures T_1 and $T_2 (T_2 > T_1)$ are prescribed at the upper and lower boundary. Using d as lengthscale, d^2/κ as timescale where κ is the thermal diffusivity, and $(T_2 - T_1) Ra^{-1}$ as scale for the temperature we write the Navier–Stokes equations in the Boussinesq approximation for the velocity vector $\boldsymbol{u}$ and the heat equation for the deviation ϑ from the temperature distribution of pure conduction in dimensionless form:

$$\nabla^2 \boldsymbol{u} + \boldsymbol{k}\vartheta - \nabla\pi = P^{-1}\left(\boldsymbol{u}\cdot\nabla\boldsymbol{u} + \frac{\partial}{\partial t}\boldsymbol{u}\right), \tag{2.1a}$$

$$\nabla\cdot\boldsymbol{u} = 0, \tag{2.1b}$$

$$\nabla^2\vartheta + Ra\,\boldsymbol{k}\cdot\boldsymbol{u} = \boldsymbol{u}\cdot\nabla\vartheta + \frac{\partial}{\partial t}\vartheta, \tag{2.1c}$$

where $\boldsymbol{k}$ is the unit vector in the vertical direction and the Rayleigh and Prandtl numbers are defined by

$$Ra = \frac{\gamma g(T_2 - T_1)d^3}{\kappa\nu}, \quad P = \frac{\nu}{\kappa}. \tag{2.2}$$

The solution of pure conduction is compatible with the solution of plane Couette flow of equations (2.1a, b),

$$\boldsymbol{u}_0 = Re\,Pzi \equiv U_0\,\boldsymbol{i} \tag{2.3}$$

where Re is the Reynolds number based on the relative velocity of the rigid plates.

As indicated in figure 1, we are assuming a Cartesian system of coordinates with the z-coordinate in the vertical direction, the x-coordinate in the direction of the applied shear, and the origin on the midplane of the layer. For more general solutions of (2.1) we introduce the representation

$$\boldsymbol{u} = U_0\,\boldsymbol{i} + U_1^{(x)}\boldsymbol{i} + U_1^{(y)}\boldsymbol{j} + \nabla\times(\nabla\times\boldsymbol{k}\phi) + \nabla\times\boldsymbol{k}\psi \equiv \boldsymbol{U} + \delta\phi + \varepsilon\psi \quad \text{with} \quad \bar{\boldsymbol{u}} = \boldsymbol{U}, \tag{2.4}$$

where the bar indicates the average over the (x, y)-plane. The component $\delta\phi$ of the velocity field is sometimes called the poloidal part while $\varepsilon\psi$ is referred to as the
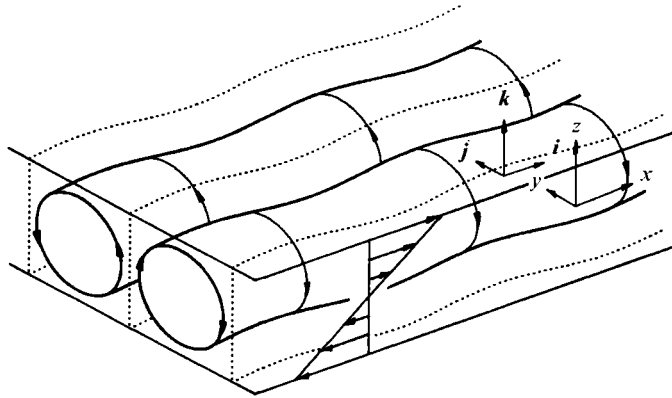
FIGURE 1. Sketch of wavy longitudinal convection rolls in a layer heated from below
in the presence of plane Couette flow.

toroidal part of the velocity field. By operating with $\boldsymbol{\delta}$ and $\boldsymbol{\varepsilon}$ onto equation (2.1c) we obtain equations for ϕ and ψ:

$$\nabla^4 \Delta_2 \phi - \Delta_2 \vartheta = P^{-1}\{\boldsymbol{\delta} \cdot [(\boldsymbol{\delta}\phi + \boldsymbol{\varepsilon}\psi) \cdot \boldsymbol{\nabla}(\boldsymbol{\delta}\phi + \boldsymbol{\varepsilon}\psi)] + (\boldsymbol{U} \cdot \boldsymbol{\nabla} + \partial_t) \nabla^2 \Delta_2 \phi - \partial_{zz}^2 \boldsymbol{U} \cdot \boldsymbol{\nabla}\Delta_2 \phi\}, \tag{2.5a}$$

$$\nabla^2 \Delta_2 \psi = P^{-1}(\boldsymbol{\varepsilon} \cdot [(\boldsymbol{\delta}\phi + \boldsymbol{\varepsilon}\psi) \cdot \boldsymbol{\nabla}(\boldsymbol{\delta}\phi + \boldsymbol{\varepsilon}\psi)] + (\boldsymbol{U} \cdot \boldsymbol{\nabla} + \partial_t) \Delta_2 \psi - \partial_z \boldsymbol{U} \cdot \boldsymbol{\varepsilon}\Delta_2 \phi\}, \tag{2.5b}$$

$$\nabla^2 \vartheta - Ra\, \Delta_2 \phi = (\boldsymbol{\delta}\phi + \boldsymbol{\varepsilon}\psi) \cdot \boldsymbol{\nabla}\vartheta + (\boldsymbol{U} \cdot \boldsymbol{\nabla} + \partial_t)\, \vartheta. \tag{2.5c}$$

We have also rewritten equation (2.1c) in the form (2.5c). In addition equations for the components $U_1^{(x,\,y)}$ of the mean field $\boldsymbol{U}(z,t)$ are needed,

$$(\partial_{zz}^2 - P^{-1}\partial_t)\, U_1^{(x)} = -\partial_z \overline{(\Delta_2 \phi(\partial_{xz}^2 \phi + \partial_y \psi))}\, P^{-1}, \tag{2.5d}$$

$$(\partial_{zz}^2 - P^{-1}\partial_t)\, U_1^{(y)} = -\partial_z \overline{(\Delta_2 \phi(\partial_{yz}^2 \phi - \partial_x \psi))}\, P^{-1}, \tag{2.5e}$$

where the bar indicates the horizontal average and the symbol Δ_2 stands for $\nabla^2 - \partial_{zz}^2$. The boundary conditions for the variables ϕ, ψ, ϑ and $U_1^{(x,\,y)}$ are given by

$$\phi = \partial_z \phi = \psi = \vartheta = U_1^{(x)} = U_1^{(y)} = 0 \quad \text{at} \quad z = \pm\tfrac{1}{2}. \tag{2.6}$$

x-independent solutions of (2.5) in the form of steady longitudinal rolls and their instabilities have been investigated in CBK. Here attention will be focused on the three-dimensional forms of convection that originate from the wavy instability of the longitudinal rolls. Since the imaginary part of the growth rate of the wavy instability vanishes, we look for steady solutions. We use the Galerkin method for the numerical solution of (2.5) and introduce expansions in complete systems of functions for the variables ϕ, ψ, ϑ and $U_1^{(x)}$:

$$\phi = \sum_{\lambda,\,\mu,\,\nu} a_{\lambda\mu\nu} \begin{Bmatrix} \cos\lambda\alpha_x x \\ \sin\lambda\alpha_x x \end{Bmatrix} g_\nu(z)\tfrac{1}{2}[((-1)^\lambda + 1)\cos\mu\alpha_y y + ((-1)^\lambda - 1)\sin\mu\alpha_y y], \tag{2.7a}$$

$$\psi = \sum_{\lambda,\,\mu,\,\nu} c_{\lambda\mu\nu} \begin{Bmatrix} \cos\lambda\alpha_x x \\ \sin\lambda\alpha_x x \end{Bmatrix} \sin\nu\pi(z+\tfrac{1}{2})\tfrac{1}{2}[((-1)^\lambda - 1)\cos\mu\alpha_y y + ((-1)^\lambda + 1)\sin\mu\alpha_y y], \tag{2.7b}$$

$$\vartheta = \sum_{\lambda,\,\mu,\,\nu} b_{\lambda\mu\nu} \begin{Bmatrix} \cos\lambda\alpha_x x \\ \sin\lambda\alpha_x x \end{Bmatrix} \sin\nu\pi(z+\tfrac{1}{2})\tfrac{1}{2}[((-1)^\lambda + 1)\cos\mu\alpha_y y + ((-1)^\lambda - 1)\sin\mu\alpha_y y], \tag{2.7c}$$

$$U_1^{(x)} = \sum_\nu U_{1\nu} \sin 2\nu\pi(z + \tfrac{1}{2}), \qquad\qquad (2.7d)$$

where the summation runs through positive integers ν and non-negative integers μ and λ. The functions $g_\nu(z)$ satisfying the boundary conditions for ϕ were originally introduced by Chandrasekhar (1961, p. 635) and their definitions can also be found in previous work by the present authors (Clever & Busse 1975, 1977). We have incorporated in representation (2.7) the symmetry in the y-direction which is preserved in the interaction of the wavy instability with the longitudinal rolls. Another symmetry of the problem is expressed in the prescription that the upper functions in the curly bracket apply in the case of even $\mu + \nu$, while the lower functions must be chosen for odd $\mu + \nu$. This symmetry is an extension of the symmetry of longitudinal rolls corresponding to the special case $\lambda = 0$ with non-vanishing coefficients for even $\mu + \nu$ only. The x-dependence introduced by the wavy instability requires that $\sin \lambda\alpha_x x$ and $\cos \lambda\alpha_x x$ terms have opposite symmetry in the z-direction. An inspection of the nonlinear terms in (2.1) shows that the above-mentioned symmetries are indeed preserved. It can also be seen from representation (2.7) that average over x and y of the products $\Delta_2 \phi\, \partial^2\phi/\partial y\, \partial z$ and $\Delta_2 \phi\, \partial\psi/\partial x$ vanishes. There are thus no Reynolds stresses which could generate a mean flow in the y-direction.

After introducing the representations (2.7) into (2.5), multiplying them by the respective expansion functions and averaging them over the fluid layer, we obtain a system of nonlinear algebraic equations for the coefficients $a_{\lambda\mu\nu}$, $c_{\lambda\mu\nu}$, $b_{\lambda\mu\nu}$, $U_{1\nu}$. In order to solve this system by a Newton–Raphson iteration method, we must introduce a truncation procedure. The condition that all coefficients and corresponding equations with subscripts satisfying the inequality

$$\lambda + \mu + \nu > N_T \qquad\qquad (2.8)$$

are dropped from the analysis appears to provide a computationally effective truncation. A numerically obtained solution is regarded a reasonable approximation for the exact solution of the infinite system if sensitive properties such as the convective heat transport do not change by more than a few percent when N_T is replaced by $N_T - 2$. Unless indicated otherwise, $N_T = 10$ has been used for the results presented in the following sections.

The Galerkin method offers the advantage of a relatively easy way in which the stability of stationary solutions can be tested. Infinitesimal three-dimensional disturbances can be superimposed onto a steady solution of the form (2.7), an exponential time dependence of the disturbances can be assumed without loss of generality, and the growth rate can be computed as the eigenvalue of a stability matrix (Busse 1967). The stability analysis becomes particularly simple when the disturbances have the same periodicity in the horizontal dimensions as the steady solution. Since most instabilities seem to belong to this category and since computations for more general disturbances require computer resources beyond those needed for the computations of the steady solutions, we shall restrict attention to disturbances with the same basic wavenumbers α_x, α_y as those characterizing the steady solution. Accordingly the disturbances can be represented in the form

$$\tilde\phi = \sum_{\lambda\mu\nu} \tilde a_{\lambda\mu\nu} \begin{Bmatrix} \cos \lambda\alpha_x x \\ \sin \lambda\alpha_x x \end{Bmatrix} g_\nu(z) \tfrac{1}{2}[((-1)^\lambda \pm 1)\cos \mu\alpha_y y + ((-1)^\lambda \mp 1)\sin \mu\alpha_y y]\exp(\sigma t),$$

$$(2.9a)$$

$$\tilde{\psi} = \sum_{\lambda\mu\nu} \tilde{c}_{\lambda\mu\nu} \begin{Bmatrix} \cos \lambda\alpha_x x \\ \sin \lambda\alpha_x x \end{Bmatrix} \sin \nu\pi(z + \tfrac{1}{2}) \tfrac{1}{2}[((-1)^\lambda \mp 1) \cos \mu\alpha_y y$$
$$+ ((-1)^\lambda \pm 1) \sin \mu\alpha_y y] \exp(\sigma t), \quad (2.9b)$$

$$\tilde{\vartheta} = \sum_{\lambda\mu\nu} \tilde{b}_{\lambda\mu\nu} \begin{Bmatrix} \cos \lambda\alpha_x x \\ \sin \lambda\alpha_x x \end{Bmatrix} \sin \nu\pi(z + \tfrac{1}{2}) \tfrac{1}{2}[((-1)^\lambda \pm 1) \cos \mu\alpha_y y$$
$$+ ((-1)^\lambda \mp 1) \sin \mu\alpha_y y] \exp(\sigma t), \quad (2.9c)$$

$$\tilde{U}_1^{(x,y)} = \sum_\nu \tilde{U}_{1\nu}^{(x,y)} \sin \pi\nu(z + \tfrac{1}{2}) \exp(\sigma t). \quad (2.9d)$$

Because of the symmetry of the steady solution (2.7), the disturbances of the form (2.9) can be separated into four classes depending on whether the choice of the upper and lower functions in the curly brackets is the same as or opposite to the choice for the steady solution (2.7) and depending on whether the upper or lower sign is chosen in expressions (2.9 a–c). The notation used for the mean flow disturbance indicates that either an x- or a y-component may be generated by the interaction of disturbances of one of the four classes with the steady solution (2.7). In particular, a y-component $\tilde{U}_1^{(y)}$ instead of an x-component $\tilde{U}_1^{(x)}$ will be generated when the lower sign is chosen. The profiles of these mean flows will be antisymmetric or symmetric with respect to the plane $z = 0$ depending on whether the choice of the functions in the curly brackets is the same or opposite to that for the steady solution (2.7).

3. The wave instability of longitudinal rolls

Before discussing the three-dimensional wavy rolls arising from the wavy instability of two-dimensional longitudinal rolls, we would like to present some further information on this instability beyond that given by CBK. As in the case of the zigzag and the skewed varicose instabilities of convection rolls (see, for example, reviews by Busse 1978, 1981) the wavy instability sets in at the stability boundary with vanishing wavenumber α_x along the axis of the rolls. As soon as the Rayleigh number Ra_{II} of the stability boundary is exceeded, however, the wavy disturbances of maximum growth correspond to finite values of α_x as shown in figure 2. Because of this property there will be an entire range of experimentally realizable values of α_x. The value α_x seen in an experiment may depend, for instance, on the rate at which the Rayleigh number has been increased. In the computations of finite-amplitude wavy rolls we have thus chosen several values in the range $0 < \alpha_x < 2$ which appears to be the most interesting one from an experimental point of view.

Only the stability boundary of longitudinal rolls in the case of air $(P = 0.7)$ has been given by CBK. Here we add the results of computations for $P = 2.5$ as shown in figure 3. While the shape of the stability boundary is rather similar to the case $P = 0.71$ in that Ra_{II} shows little variation with the Reynolds number beyond a value of about 100, the minimum value $Ra_{II} - Ra_c$ is increased by a factor of the order 30. In this as well as in other respects longitudinal rolls with Couette flow resemble those with Poiseuille flow as has been noted in a recent study of the latter case (Clever & Busse 1991). At higher Prandtl numbers the boundary for the onset of the wavy instability moves up to higher Rayleigh numbers such that it will be preceded by other instabilities, e.g. the knot instability. Detailed studies of these cases have not yet been done.
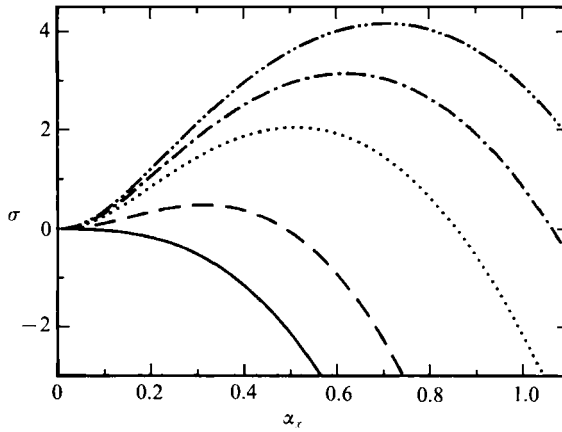
FIGURE 2. Growth rates σ of wavy disturbances of longitudinal rolls in the presence of plane Couette flow with $Re = 200$ as a function of α_x. The Rayleigh numbers are 1750, 1850, 2000, 2100, 2200 from the bottom to the top curve. The Prandtl number $P = 0.71$ and the wavenumber $\alpha_y = 3.117$ have been used.
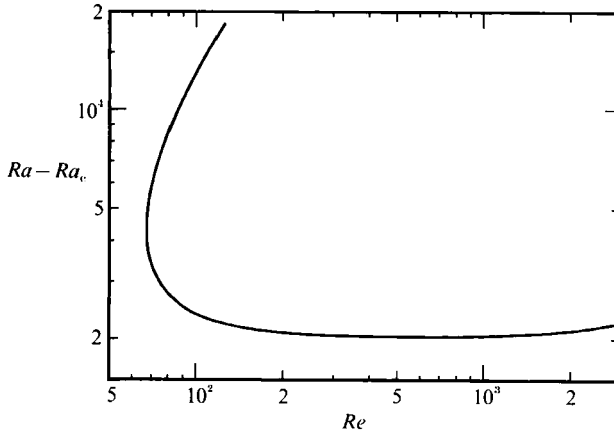

FIGURE 3. The stability boundary of longitudinal rolls in the (Re, Ra)-plane with respect to the onset of the wavy instability for $P = 2.5$, $\alpha_y = 3.117$.

4. Properties of finite-amplitude wavy rolls

While the convective heat transport and the fields ϕ and ϑ are independent of the Reynolds number for longitudinal rolls, they become strongly dependent on Re after the transition to wavy rolls has occurred. The shearing action of the Couette flow on the three-dimensional convection results in a dramatic decrease in the efficiency of heat and momentum transport by convection for Prandtl numbers around 2.5 as shown in figure 4(a). The shear Nusselt number S displayed in the figure is defined as the ratio between the momentum transport with and without convection,

$$S = 1 + \frac{\mathrm{d}U_1}{\mathrm{d}z}\bigg|_{z=\pm\frac{1}{2}} Re^{-1} = 1 - \langle \Delta_2\, \phi(\partial_{xz}^2 \phi + \partial_y \psi) \rangle\, Re^{-1}, \tag{4.1}$$

where the angular brackets indicate the average over the fluid layer. For longitudinal rolls $\partial_x \phi$ vanishes and ψ is proportional to Re has been shown in CBK. The shear
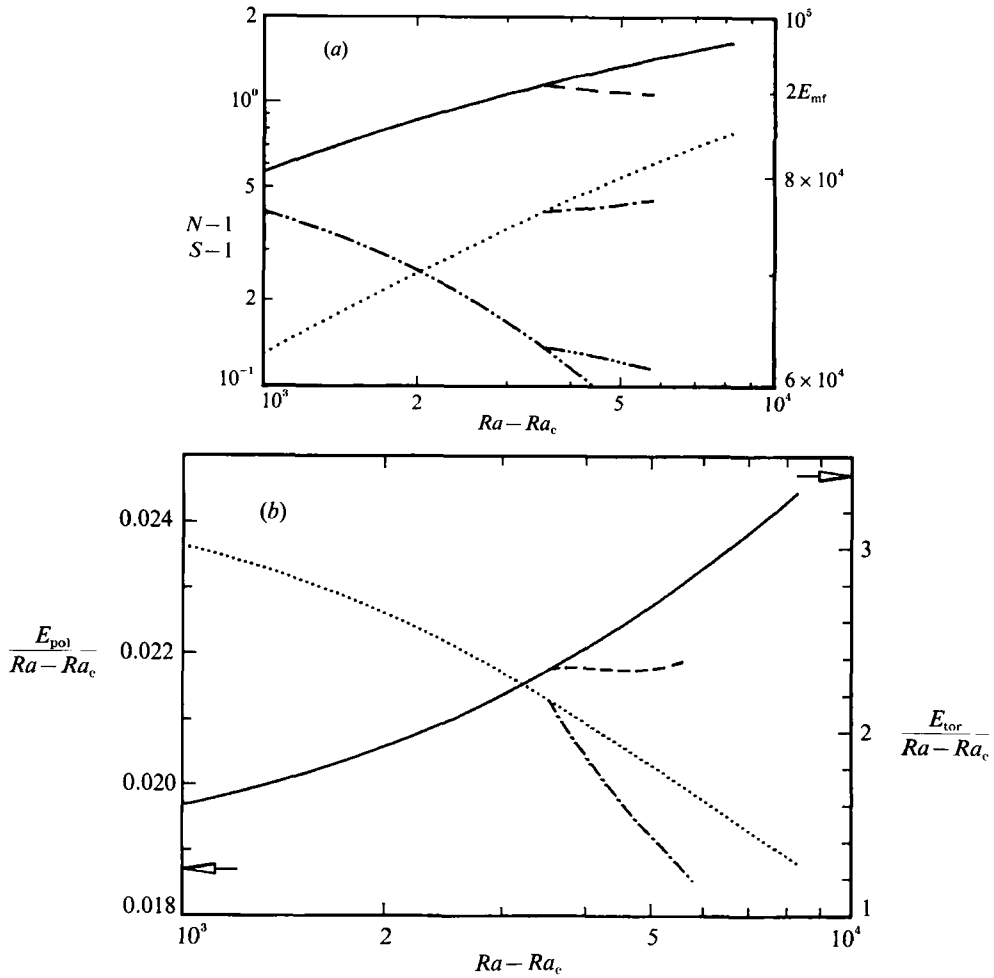
FIGURE 4. (a) Heat transport (——) and shear (......) Nusselt numbers, N and S, as function of the Rayleigh number. Also shown is the mean flow energy, E_{mf} (—·——··), corresponding to the right ordinate. The curves for the wavy rolls with $\alpha_x = 0.6$ bifurcate from the corresponding curves for two-dimensional longitudinal rolls. All curves have been computed for $P = 2.5$, $\alpha_y = 3.117$, $Re = 400$. (b) The kinetic energies of the poloidal (——) and toroidal (......) components of the fluctuating velocity field have been plotted for the same case as (a). The arrows indicate limiting values for $Ra = Ra_c$.

Nusselt number is thus independent of the Reynolds number. The heat transport Nusselt number N obeys its usual definition

$$N-1 = -Ra^{-1}\frac{\mathrm{d}}{\mathrm{d}z}\vartheta\,|_{z=\pm\frac{1}{2}}. \tag{4.2}$$

Also shown in figure 4(a) is the kinetic energy of the mean flow,

$$E_{mf} \equiv \frac{1}{2}\int_{-\frac{1}{2}}^{\frac{1}{2}} U^2\,\mathrm{d}z \tag{4.3}$$

which decreases with increasing Rayleigh number, because convection converts mean flow energy into energy of the spatially fluctuating motion. This decrease is weakened by the onset of the wavy rolls with their less efficient transport properties.
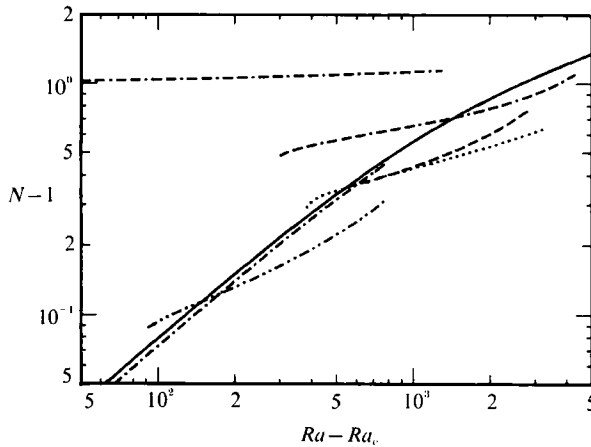
FIGURE 5. The heat transport Nusselt number N as a function of the Rayleigh number for two-dimensional rolls with $P = 0.71$ (———) and $P = 0.3$ (—·—·—) and for wavy rolls with $P = 0.71$, $Re = 200$, $\alpha_x = 1.3$ (———); $P = 0.71$, $Re = 400$, $\alpha_x = 0.9$ (......) and $\alpha_x = 1.5$ (—— ·——); $P = 0.71$, $Re = 700$, $\alpha_x = 2.0$ (—— ·——); and $P = 0.3$, $Re = 200$, $\alpha_x = 1.2$ (—··——··). In all cases $\alpha_y = 3.117$ has been used.

The post-bifurcation decrease of the Nusselt number is associated with a decrease of the amplitude of convection as measured by the kinetic energy of the poloidal component of motion,

$$E_{\rm pol} \equiv \tfrac{1}{2}\langle |\nabla \times (\nabla \times k\phi)|^2 \rangle. \tag{4.4}$$

The toroidal component of motion does not contribute to the heat transport, but it is strongly involved in the momentum transport according to relationship $(2.5d)$. The toroidal kinetic energy

$$E_{\rm tor} = \tfrac{1}{2}\langle |\nabla \times k\psi|^2 \rangle \tag{4.5}$$

is plotted together with $E_{\rm pol}$ in figure $4(b)$.

The transition to three-dimensional wavy rolls becomes more complicated as the Prandtl number is lowered. As shown in figures 5 and 6 some of the curves for three-dimensional convection are not connected with those for two-dimensional convection because subcritical bifurcations typically occur at higher values of the Reynolds number. With the numerical method used in the present analysis it has not been possible to compute the unstable branch connected with the bifurcation points on the curves for longitudinal rolls. For low Reynolds numbers, such as the case $Re = 200$, $\alpha_x = 1.3$, $P = 0.71$ of figures 5 and 6 the bifurcation still occurs supercritically. But for large Reynolds numbers and wavenumbers the subcritical character of the bifurcation becomes increasingly noticeable. In the case of the highest Reynolds number, $Re = 700$, shown in figures 5 and 6(a) the Nusselt numbers N and S become almost independent of the Rayleigh number indicating a shear-driven mechanism for the generation of three-dimensional motion. This phenomenon will be discussed in more detail in the following section.

Figure 7 gives an impression of the flow field of the wavy rolls. Since a solution removed from the point of bifurcation has been selected, the velocity field differs significantly from the simple sinusoidal distortion of the longitudinal rolls at the onset of instability. It is interesting to note that the distortion of the lines of constant vertical velocity becomes quite small in the midplane of the layer compared to the regions above and below. Only the isotherms continue to exhibit strong distortions even in the midplane as the Reynolds number is increased. The vertical velocity in
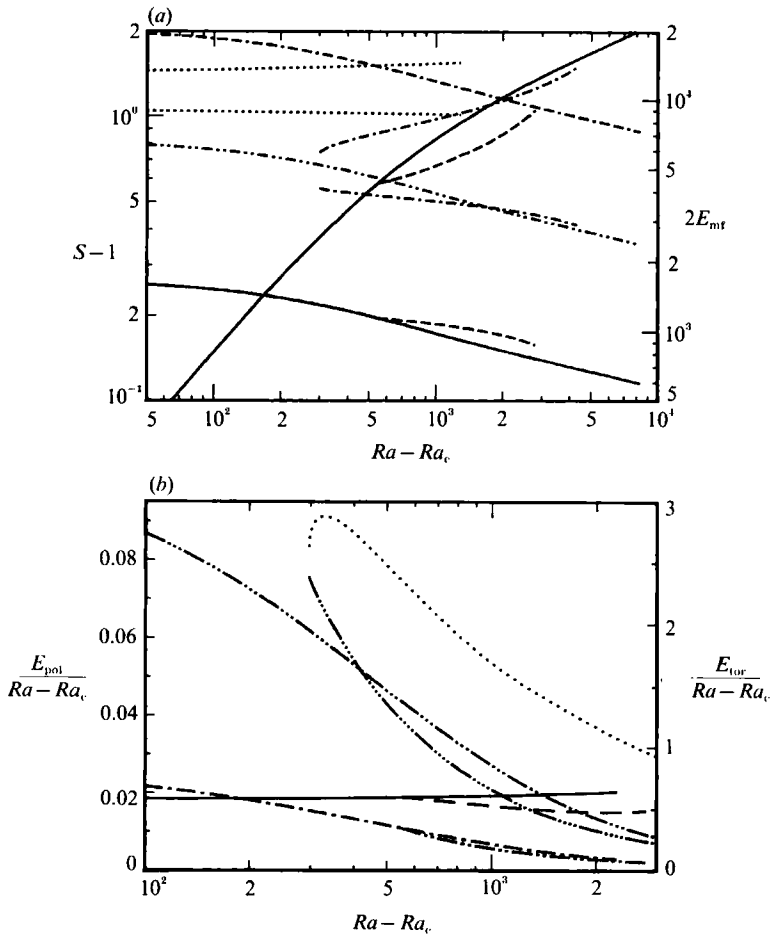
FIGURE 6. (a) Shear Nusselt number S (left ordinate, ascending curves) and kinetic energy of the mean flow (right ordinate, descending curves) as function of the Rayleigh number. The cases of two-dimensional longitudinal rolls for $Re = 200$ (———) with bifurcating wavy rolls with $\alpha_x = 1.3$ (———) and the same case for $Re = 400$ with $\alpha_x = 1.5$ (—··—··, —·—·—) and for $Re = 700$ with $\alpha_x = 2.0$ (—––·—·, ······) are shown. $P = 0.71$, $\alpha_y = 3.117$ are used in all cases. Note that S is independent of Re. (b) The kinetic energies of the poloidal (———) and toroidal (—·—·—, —···—···) components of the fluctuating velocity field in the case of two-dimensional longitudinal rolls with $Re = 200$ and $Re = 400$. Also shown are the cases of wavy rolls with $Re = 200$, $\alpha_x = 1.3$ (————, E_{pol}; —···—··, E_{tor}) and $Re = 400$, $\alpha_x = 1.5$ (······, E_{pol}; —····—, E_{tor}). $P = 0.71$, $\alpha_y = 3.117$ are used in all cases.

the midplane is thus not representative of the velocity field and more interesting information can be obtained from isolines in planes closer to boundaries such as $z = \pm 0.3$.

The decrease of the kinetic energy of the mean flow with increasing Rayleigh number is reflected in the change of the profile of the mean flow shown in figure 8. It is apparent that two-dimensional longitudinal rolls exert a stronger influence on the mean shear than three-dimensional wavy rolls at the same Rayleigh number. This property is especially evident from a comparison of the two profiles for $Ra = 2500$.
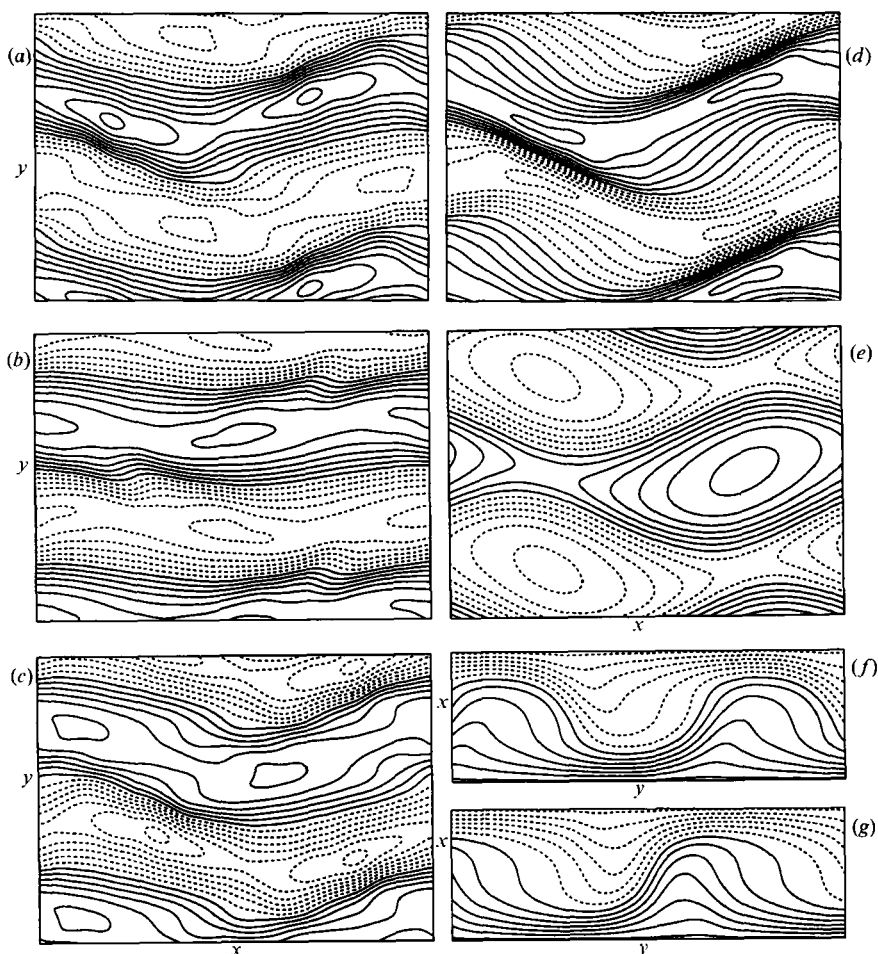
FIGURE 7. Lines of constant vertical velocity in the plane (a) $z = 0.3$, (b) $z = 0$ and (c) $z = -0.3$; and (d) isotherms and (e) streamlines $\psi = $ const. in the plane $z = 0$. The isotherms in the planes (f) $x = 0$ and (g) $x = \pi/2\alpha_x$ are shown also. All plots correspond to the case $Ra = 3000$, $Re = 400$, $P = 0.71$, $\alpha_x = 1.5$, $\alpha_y = 3.117$. Broken lines indicate negative values, solid lines positive values except for the line adjacent to the broken lines which indicates zero.

5. Finite-amplitude solutions of vanishing or negative Rayleigh numbers

The question of secondary solutions in the case of plane Couette flow of a homogeneous fluid has long fascinated fluid dynamicists. It has become evident through the work of many researchers that there does not exist a finite Reynolds number at which a secondary solution bifurcates from the basic solution of constant shear. Turbulent motions have been observed in experiments at Reynolds numbers as low as $Re = 1000$ (Reichardt 1959) and time-dependent solutions for the problem have been obtained numerically by Orszag & Patera (1983). Recently Nagata (1990) has obtained numerically steady three-dimensional solutions for the plane Couette flow problem. He has considered the problem of plane Couette flow in a rotating system for which secondary solutions describing Taylor vortices and more complex flows can easily be obtained. By changing the rotation parameter to zero Nagata was able to reach the case of plane Couette flow.

In the present problem we follow a similar procedure. By extending the subcritical solutions found in the case of air $(P = 0.71)$ to low Rayleigh numbers we find three-
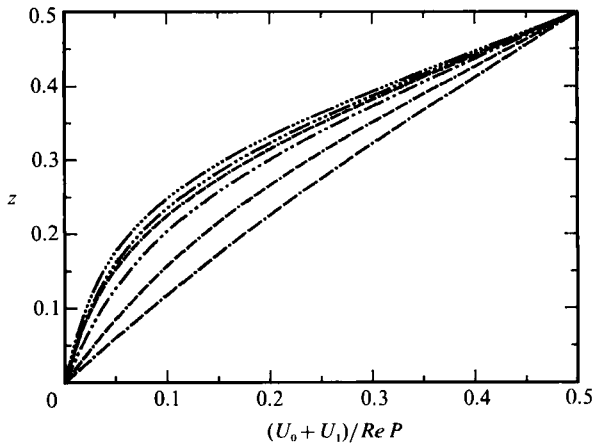
FIGURE 8. Mean flow profiles normalized with the Reynolds number. They are shown for $z > 0$ only because of their antisymmetry with respect to $z = 0$. $Re = 400$, $P = 0.71$ and $\alpha_y = 3.117$ have been assumed in all cases: —–·—– $(Ra = 1800)$, ——·——· $(Ra = 2000)$ and ————·——— $(Ra = 2500)$ correspond to longitudinal rolls; —–··—··, $(Ra = 2500)$, —–···——··· $(Ra = 4000)$ and —–····—···· $(Ra = 5000)$ correspond to wavy rolls with $\alpha_x = 0.9$.
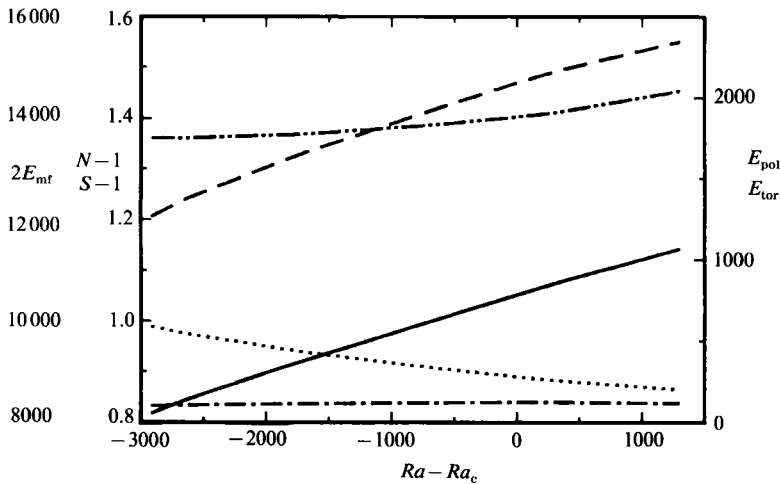
FIGURE 9. Heat transport Nusselt number N (———), shear Nusselt number S (———) and kinetic energies of the mean flow, E_{mf} (……), of the poloidal component, E_{pol} (—–·—–·—), and of the toroidal component, E_{tor} (—–··—··), as functions of the Rayleigh number for $Re = 700$, $P = 0.71$, $\alpha_x = 2.0$ and $\alpha_y = 3.117$. $N_T = 12$ has been used for these computations.

dimensional wavy roll solutions of the same kind as those of Nagata (1990). In figure 9 the smooth dependence of the properties of wavy rolls is evident as the Rayleigh number is decreased to negative values for a sufficiently high prescribed Reynolds number. The solutions appear to be well converged if a sufficiently high truncation parameter has been chosen. $N_T = 12$ has been used for the solutions plotted in figure 9. Only towards the low-Rayleigh-number limit of their existence does a sensitive dependence on N_T becomes noticeable. In the case of figure 9 this limit lies somewhat below -3000. Of particular interest are properties of solutions in the isothermal case shown in figure 10 for two different Reynolds numbers. As is evident from the plots, the flow does not differ significantly from the flow in the unstably stratified case of figure 7 except that more small-scale structure becomes noticeable, especially in the
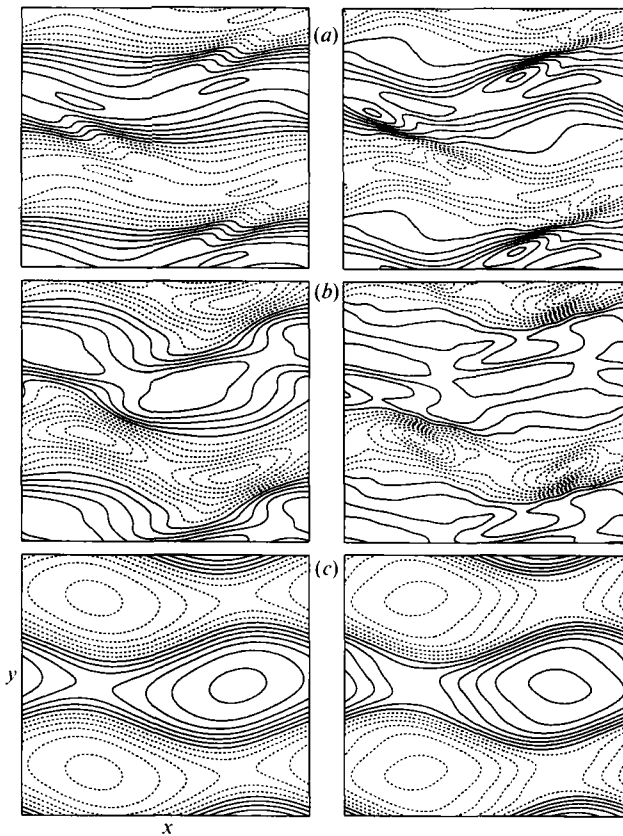
FIGURE 10. Lines of constant vertical velocity in the planes (a) $z = 0$ and (b) $z = -0.3$, and (c) lines of constant $\psi(x, y)$ in the plane $z = 0$. All plots correspond to $Ra = 0$, $\alpha_x = 1.5$, $\alpha_y = 2.5$. Left and right plots respectively correspond to $Re = 590$ and $Re = 1000$. $N_T = 16$ has been used for the computations.
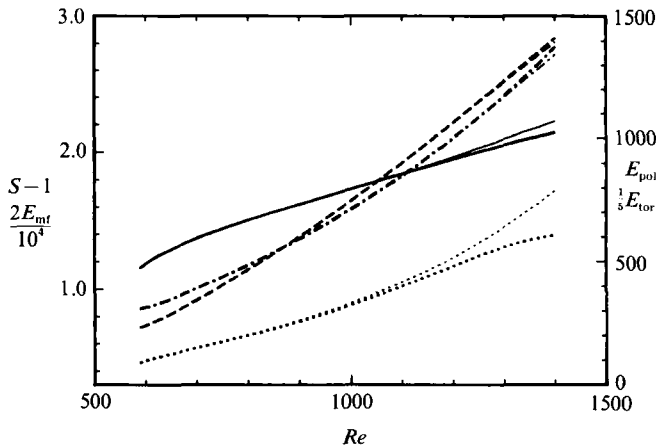

FIGURE 11. Shear Nusselt number S (———) and kinetic energies of the mean flow, E_{mf} (————), and of the poloidal and the toroidal components of the velocity field, E_{pol} (......) and E_{tor}(—·—·—), as functions of the Reynolds number for $P = 0.71$, $Ra = 1$, $\alpha_x = 1.5$ and $\alpha_y = 3.117$. Thick lines have been computed with $N_T = 16$, thin lines correspond to $N_T = 14$.
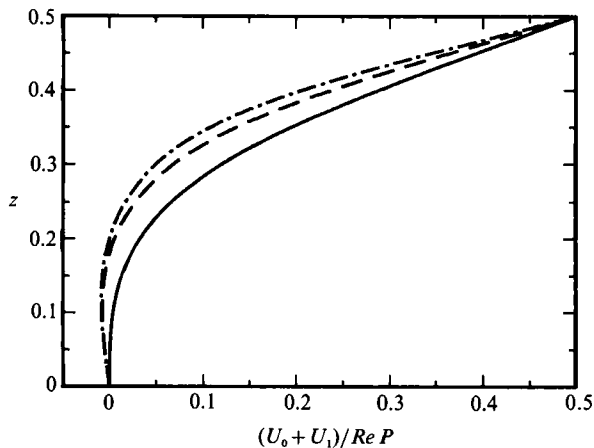
FIGURE 12. Mean flow profiles normalized with the Reynolds number in the case of wavy rolls with $Re = 590, 1000, 1400$ (from bottom to top). $P = 0.71$, $Ra = 0$, $\alpha_x = 1.5$, $\alpha_y = 2.5$ have been used in the computations.

high-Reynolds-number case. The variation of the averaged properties with the Reynolds number is shown in figure 11. For numerical reasons $Ra = 1$ has been chosen in this figure instead of $Ra = 0$, but this small difference has a negligible influence on the solutions. Since the numerical accuracy of the Galerkin scheme deteriorates towards high Reynolds number, we have used $N_T = 16$ for the computations and show results obtained with $N_T = 14$ for comparison.

Finally some mean flow profiles are shown in figure 12 for this Reynolds-number range. The deviations of these profiles from the linear profile (2.3) of the basic state are more pronounced than in the cases shown in figure 8. The slope of the profile at the midplane of the layer even reverses except in the case of the lowest Reynolds number. In this respect the profiles resemble that of the mean temperature for two-dimensional convection rolls in Rayleigh–Bénard convection (see, for example, Busse 1978).

6. Instabilities of wavy convection rolls

In addition to the solutions with large values of α_x discussed in the two preceding sections a large number of wavy roll solutions with lower values of α_x have been computed. They have not been considered in this paper since they usually were found to be unstable even close to their onset in the case of supercritical bifurcation. Even the solutions that have been discussed in the preceding section have been found to be unstable to a large extent. For example for $P = 2.5$ wavy roll solutions were obtained for $\alpha_x = 0.2$, 0.4 and 0.6. But all solutions are unstable with respect to growing disturbances that differ in symmetry from the steady wavy roll solution. The imaginary part of the growth rate corresponds roughly to $\pm \frac{1}{3}\alpha_x Re$ which indicates that the disturbances tend to have their maximum amplitude close to one of the boundaries and are advected by the mean flow. There is a tendency towards stability with increasing α_x, but for $P = 2.5$ we have not succeeded in obtaining a converged solution for values of α_x significantly larger than 0.6.

The most important instability of steady wavy rolls at lower Prandtl numbers assumes the form of disturbances with the same spatial symmetry as that of expressions (2.7). This feature is surprising since instabilities usually tend to break a spatial symmetry of the steady flow. In the present case the symmetry in time is
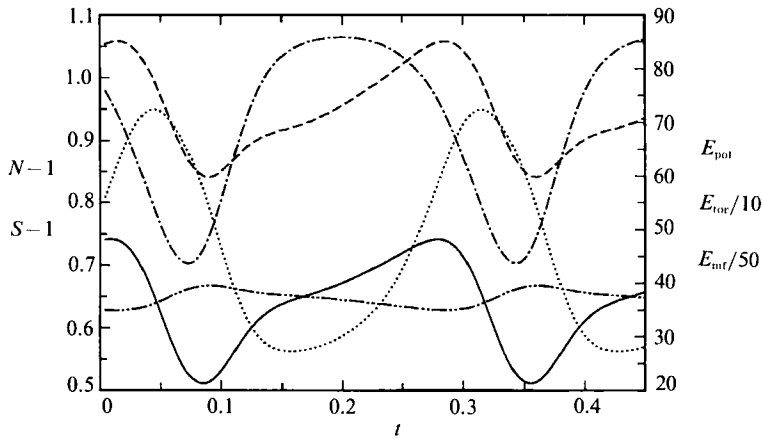
FIGURE 13. Nusselt number N (———), shear Nusselt number S (———), kinetic energies of the poloidal (......), toroidal (—·—·—) and mean (—··—··—) components of the velocity field for the vacillating wavy roll solution as a function of time t. $Ra = 3000$, $P = 0.71$, $\alpha_x = 1.5$, $\alpha_y = 3.117$ and $N_T = 8$ have been used in the computations.

broken in that the growth rate exhibits a finite imaginary part. Since similar instabilities are known from rotating systems – we refer to the amplitude vacillations in the rotating annulus experiment (Pfeffer & Chiang 1967) and to vacillations of centrifugally induced convection (Or & Busse 1987) – we shall call this instability the vacillation instability. The imaginary part σ_i is usually small compared to $\alpha_x Re$ and does not scale with this latter parameter. Nor does there seem to exist a clear relationship with Ra. The order of magnitude of the oscillation period corresponds roughly to the circulation time of the rolls and the vacillations thus appear to be similar to the oscillations found by Domaradzki & Metcalfe (1988) at a similar Reynolds number, but with a 10 times higher Rayleigh number. In the case of air with $Re = 700$ this instability occurs throughout the entire branch of the wavy roll solution and all solutions obtained for $Ra \approx 0$ are also unstable. In this latter case σ_i increases from about 10 at $Re = 580$ to about 30 at $Re = 800$ in the case $\alpha_x = 1.5$, $\alpha_y = 2.5$.

For air with $Re = 400$ the vacillation instability occurs for $Ra - Ra_c \geqslant 570$ when $\alpha_x = 1.5$ and for $Ra - Ra_c \geqslant 390$ when $\alpha_x = 0.9$. But in the latter case it is preceded by an instability which exhibits symmetries opposite to that of the steady solution in both respects as discussed in connection with (2.9). In the case of $Re = 200$ with $\alpha_x = 1.3$ the vacillation instability sets in at $Ra - Ra_c = 1400$. Only in the case of $P = 0.3, \alpha_x = 1.2$ no instability was found throughout the range for which the wavy roll solution has been computed.

The property that the vacillation instability does not change the spatial symmetry of the wavy roll solutions permits a relatively straightforward computation of the evolution in time of the flow. Assuming time-dependent instead of constant coefficients in the representation (2.7) we use a semi-implicit Crank–Nicholson scheme for the forward integration in time. After a few periods of approximate length $2\pi/\sigma_i$ the flow settles into a limit cycle as shown for $Ra = 3000$ in figure 13. The vacillation occurs between a nearly two-dimensional state of longitudinal rolls with efficient transports as indicated by the high values of S and N and a three-dimensional state of strongly distorted rolls in which kinetic energy of the toroidal component of flow is converted into kinetic energy of the poloidal component. The sequence of pictures shown in figure 14 demonstrates this striking change. The latter
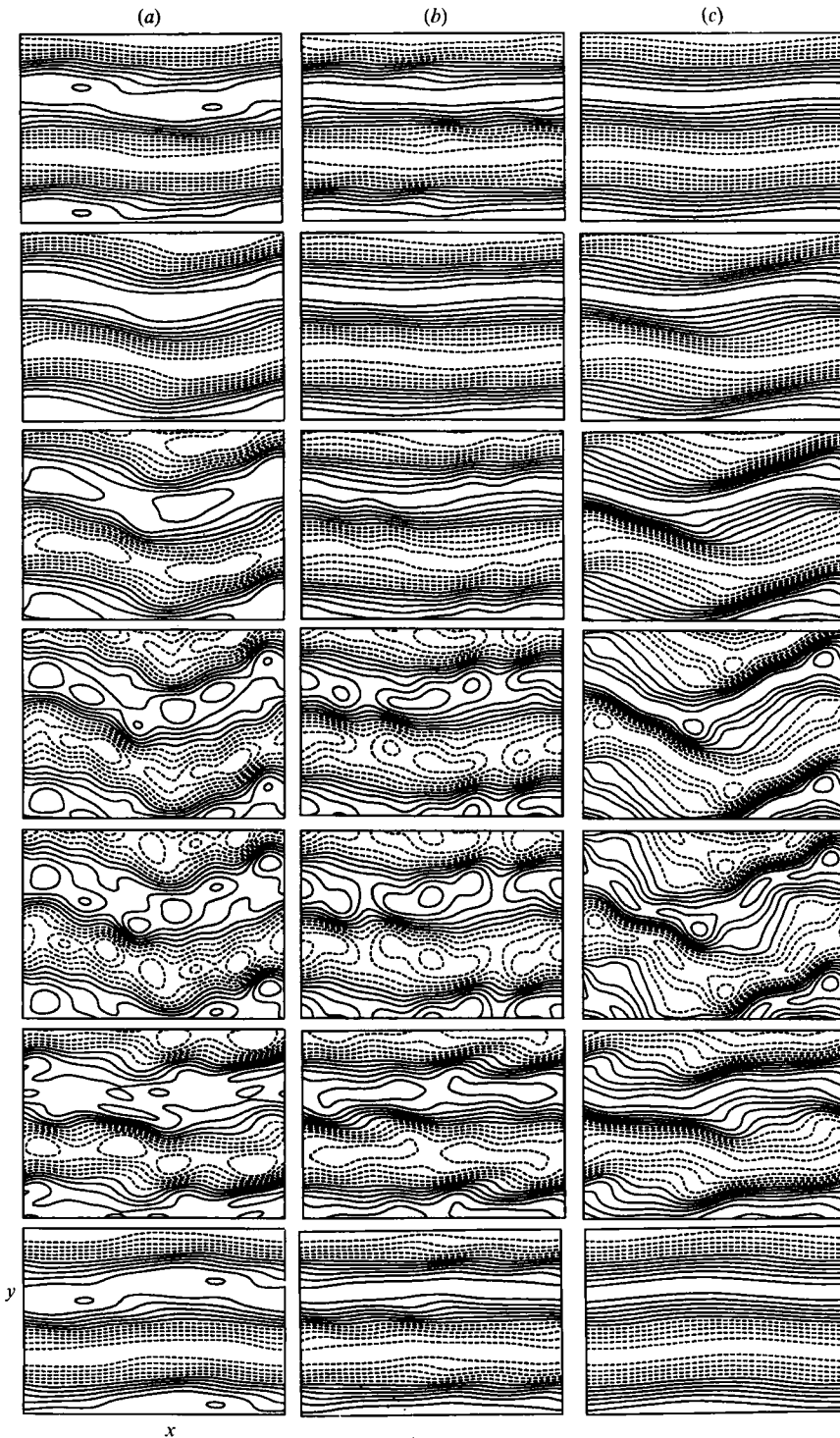
FIGURE 14. Lines of constant vertical velocity at (a) $z = -0.3$ and at (b) $z = 0$ and (c) lines of constant temperature at $z = 0$ are shown at equal time steps from $t = 0.1575$ (top row) to $t = 0.4275$ (bottom row) for the solution plotted in figure 13. This time interval corresponds approximately to a half-cycle of the vacillation. Solid (broken) lines indicate positive (negative) values except for the solid line adjacent to the broken lines which indicates zero.

state resembles the state of three-dimensional wavy rolls shown in figure 7 except that the distortions appear to be amplified. It can also be seen that the period exhibited by the mean properties in figure 13 corresponds to the half-period of the limit cycle since the process of three-dimensional distortion shifts back and forth by half a wavelength in the x-direction in each period.

The evolution of the vacillation instability for $Ra \approx 0$ has also been studied. In these cases, however, a limit cycle does not seem to exist and the solution approaches the solution of pure Couette flow, $\phi \equiv \vartheta \equiv \psi \equiv 0$, asymptotically. From our preliminary study of time-dependent states it thus appears that a stable simple secondary solution does not exist in the homogeneous case $Ra = 0$.

7. Concluding remarks

It is evident from the results presented in §§4 and 5 that the problem of the interaction between thermal convection and a mean shear is a complex one even in the case of the steady three-dimensional wavy roll solutions. At sufficiently low values of the Reynolds number the effect of the shear on the convection is minimal. As long as longitudinal rolls are realized the heat transport and the kinetic energy of the poloidal part of the velocity field are independent of the Reynolds number. The shear may even contribute to the efficiency of the heat transport by delaying the onset of instabilities which usually tend to decrease the efficiency of convection.

At somewhat larger values of Re the wavy instability sets in supercritically and leads to diminished transport in comparison with the longitudinal roll solutions. At higher values of Re or, more accurately, of $\alpha_x Re$, energy of the mean flow is not only transferred into the toroidal fluctuating component of motion (as in the case of longitudinal rolls), but also into the poloidal component. An enhancement of the heat and momentum transport is associated with the latter process which gives rise to significant convective transport at Rayleigh numbers even below the critical value of onset of convection. Nevertheless, at high Rayleigh numbers the disrupting influence of the shear-induced motions still leads to lower transport than those associated with longitudinal rolls.

The steady wavy roll solutions are stable with respect to disturbances which do not change the horizontal periodicity interval only for a limited range of Rayleigh numbers. Tertiary instabilities lead to time-dependent states, in general. Only preliminary investigations of these states have been done. Of particular interest is the vacillating state in which the fluid flow appears to oscillate between the longitudinal roll state and a highly distorted wavy roll state. This property as well as properties of the steady wavy roll solutions appear to be remarkably robust since they can be noticed in the turbulent regime at high Rayleigh numbers studied in the numerical simulations of Domaradzki & Metcalfe (1988).

REFERENCES

Asai, T. 1970 Three-dimensional features of thermal convection in a plane Couette flow. *J. Met. Soc. Japan* **48**, 18–29.

Busse, F. H. 1967 On the stability of two-dimensional convection in a layer heated from below. *J. Math. Phys.* **46**, 140–150.

BUSSE, F. H. 1978 Nonlinear properties of convection. *Rep. Prog. Phys.* **41**, 1929–1967.

BUSSE, F. H. 1981 Transition to turbulence in Rayleigh–Bénard convection. Chapter 5. In *Hydrodynamic Instabilities and the Transition to Turbulence* (ed. H. L. Swinney & J. P. Gollub), chap. 5. Springer.

CHANDRASEKHAR, S. 1961 *Hydrodynamic and Hydromagnetic Stability*. Clarendon.

CLEVER, R. M. & BUSSE, F. H. 1974 Transition to time-dependent convection. *J. Fluid Mech.* **65**, 625–645.

CLEVER, R. M. & BUSSE, F. H. 1977 Instability of longitudinal convection rolls in an inclined layer. *J. Fluid Mech.* **81**, 107–127.

CLEVER, R. M. & BUSSE, F. H. 1991 Instabilities of longitudinal rolls in the presence of Poiseuille flow. *J. Fluid Mech.* **229**, 517–529.

CLEVER, R. M., BUSSE, F. H. & KELLY, R. E. 1977 Instabilities of longitudinal convection rolls in Couette flow. *Z. Angew. Math. Phys.* **28**, 771–783 (referred to herein as CBK).

DOMARADZKI, J. A. & METCALFE, R. W. 1988 Direct numerical simulations of the effects of shear on turbulent Rayleigh–Bénard convection. *J. Fluid Mech.* **193**, 499–531.

GALLAGHER, A. P. & MERCER, A. McD. 1965 On the behaviour of small disturbances in plane Couette flow with a temperature gradient. *Proc. R. Soc. Lond.* A **286**, 117–128.

KUETTNER, J. P. 1971 Cloud bands in the Earth's atmosphere. *Tellus* **23**, 404–425.

NAGATA, M. 1990 Three-dimensional finite amplitude solutions in plane Couette flow: bifurcation from infinity. *J. Fluid Mech.* **217**, 519–527.

OR, A. C. & BUSSE, F. H. 1987 Convection in a rotating cylindrical annulus. Part 2. Transition to symmetric and vacillating flow. *J. Fluid Mech.* **174**, 313–326.

ORSZAG, S. A. & PATERA, A. T. 1983 Secondary instability of wall-bounded shear flows. *J. Fluid Mech.* **128**, 347–385.

PFEFFER, R. L. & CHIANG, Y. 1967 Two kinds of vacillation in rotating laboratory experiments. *Mon. Weath. Rev.* **95**, 75–82.

REICHARDT, H. 1959 Gesetzmäßigkeiten der geradlinigen turbulenten Couetteströmung. *Mitt. Max-Planck-Institut für Strömungsforschung, Göttingen*, Nr. 22.